Crystal transformation from the incorporation of coordinate bonds into a hydrogen-bonded network yields robust free-standing supramolecular membranes

*Peng Meng, Aidan Brock, Yanan Xu, Chenhui Han, Su Chen, Cheng Yan, John McMurtrie and Jingsan Xu**

School of Chemistry, Physics and Mechanical Engineering, Science and Engineering Faculty, Queensland University of Technology, Brisbane, QLD 4001, Australia

Abstract: In this work, we report on the synthesis of a free-standing, macroscopic robust supramolecular membrane by introducing silver-nitrogen coordinate bonding into pre-organized, supramolecular hydrogen-bonded cyanuric acid-melamine (CAM) crystals. With the assistance of ammonia, silver ions competitively replace two of the three hydrogen atoms from cyanuric acid resulting in the transformation from short CAM nanorods to long CAM-Ag nanofibers (length over 1000 μm), accompanied by tautomerization of cyanuric acid. The single crystal structure of the CAM-Ag nanofibers is solved in the space group *P*1, with the asymmetric unit containing eight silver atoms, four melamine and four cyanuric acid molecules, which generate 1D coordination polymer chains consisting of alternating melamine and dianionic cyanurate ligands linked *via* silver-nitrogen bonds. The presence of inter-chain hydrogen bonds results in the expansion of the supramolecular network into undulating 2D sheets, which then stack into a 3D network via a series of inter-sheet hydrogen bonds and π-π interactions. Significantly, the CAM-Ag nanofibers spontaneously assemble into a free-standing membrane, with lateral size up to square centimeters and thickness of 30 micrometers. The membrane shows high flexibility and mechanical strength, owing to the improved flexibility of the CAM-Ag nanofibers with bonded chain structure, and can be reversibly and repeatedly bent over 90 degrees. Remarkably, the CAM-Ag membrane

demonstrates distinct optical transmittance being shortwave IR transmissive but impenetrable to UV and visible light.

1. Introduction

Over the past few decades, supramolecular self-assembly has been a field of intensive interest owing to potential applications in separation, biosensing and energy conversion, *etc*.[1] The most common intermolecular interactions within supermolecules include coordination, hydrogen bonding and *van der Waals* interaction, π-π interactions, *etc*. Normally, supramolecular materials based on coordinate bonds have higher chemical strength than those connected by noncovalent bonds; hydrogen bonds which are strong may have energy comparable to coordinate bonds (~100 kJ/mol), while the energy of *van der Waals* forces is much lower (~10 kJ/mol). The relatively weak interactions, on the one hand, endow supermolecules remarkable functionalities with high flexibility and reversibility and demonstrate potential applications in sensing, smart materials and catalysis.[2-4] And, on the other hand, due to the weak connection of noncovalent bonds, supramolecular aggregates are usually limited to nano- or micro-meter scales and have relatively poor mechanical strength,[3, 5-6] which hinders their practical application. To date, the search for macro-scale, highly accessible supramolecular materials is of great interest and remains a challenging task.

Functional supramolecular membranes, namely 2D architectures made of supermolecules, have attracted increasing attention due to the potential for application in desalination,[7-8] therapy[9] and efficient energy conversion.[10-11] However, fabricated supramolecular membranes are typically fragile and thus require substrates for support, or to be mixed with materials (*e.g.* graphene) for improved mechanical strength.[12-16] Several groups have recently developed a self-assembly strategy at water/air and liquid/liquid interfaces to synthesize free-standing, 2D supramolecular sheets.[10, 17-20] Nevertheless, the lateral sizes were limited to the range of microns-to-millimeters. Moreover, the supramolecular sheets ranged from

nanometer to atomic thickness and so special techniques and great care were required for materials transfer, measurements and subsequent applications. Some researchers have fabricated large-size membranes assembled from nanocrystals of perylene diimide dye and its derivatives.[21-22] However, it is still highly challenging to design and synthesize robust and macroscopic supramolecular membranes with desirable mechanical, optical and other functions.

Cyanuric acid-melamine (CAM) complex is one classic supramolecular assembly that is connected by hydrogen bonds (O···H-N and N-H···N), resulting in hexamers that are arranged in planar sheets stacked in three dimensions.[23-24] The CAM framework can serve as an excellent platform for constructing more complex supramolecular architectures by introducing other hydrogen-bond donors or acceptors.[25] Recently, it was used as a remarkable precursor for synthesizing polymeric carbon nitride (a metal-free semiconductor) for improved photocatalytic water splitting.[26-28] In addition, it has been well recognized that Ag(I) can readily form coordinate bonds with nitrogen-donors including triazine, pyridyl and many others to drive assembly of different nanostructures.[2,29-31] A linear, two coordinate, coordination geometry is generally preferred between Ag(I) and the N-donors. Inspired by these facts, we have herein successfully incorporated Ag-N coordinate bonds into H-bonded CAM supramolecular nanorods, leading to the formation of CAM-Ag nanofibers with a chain-like structure. Unlike the conventional "bottom-up" strategy for building supramolecular crystals by connecting pre-formed coordination subunits with relatively weaker hydrogen bonds,[32-33] H-bonded CAM crystals were firstly generated and the hydrogen atoms were then competitively substituted by Ag(I), which form coordinate bonds alternatingly with melamine and cyanuric acid. Interestingly, the resulting CAM-Ag nanofibers, with a large aspect ratio of up to 10000, spontaneously assemble into a highly flexible, self-supported supramolecular membrane with lateral size in the centimeter range.

The membrane demonstrates unique selective optical transmission, *i.e.*, shortwave IR transmissive but UV and visible light impenetrable.

2. Results and Discussion

2.1. Synthesis of CAM-Ag nanofibers and membranes

As aforementioned, the planar CAM lattice is held together by O···H-N and N-H···N hydrogen bonds (Figure 1a). The CAM dispersion was prepared by mixing an aqueous solution of cyanuric acid and melamine with equal concentration and volume (20 mM, 0.5 mL). $AgNO_3$ solution was then added to initiate the next-step reaction (Figure 1b), wherein the Ag(I) concentration was set to be 10 mM in the solution. The system was kept still under ambient environment for the generation of Ag-incorporated materials. The morphologies of the precipitated products were observed after different time intervals. SEM images show that the pristine CAM product was composed of irregular nanorods (Figure 1c, CAM), agreeing with a previous report.[26] After 3 h in the presence of Ag(I), a very small number of nanofibers were formed, as illustrated by the arrows in Figure 1c (Ag-3h). The nanofibers were much longer (1000 μm) and thinner (100 nm) than the CAM nanorods. The nanofibers became more pronounced when the standing time was prolonged to 6 and then 24 h. The number of nanofibers remained unchanged upon further standing (up to several days). Additionally, silver was found to be present in the nanofibers, as demonstrated by the back-scattered electron mapping (Figure 1d) and the corresponding energy dispersive scanning (EDS) mapping (Figure S1). These results suggest the generation of a new, silver-containing phase, which can also be verified by powder X-ray diffraction (PXRD) shown in Figure 3a. In comparison to the diffraction pattern of CAM, several new diffraction peaks can be clearly resolved which are assigned to the emerged nanofibers. The crystal transformation was incomplete, as indicated by the presence of the short nanorods and diffraction peaks from CAM.

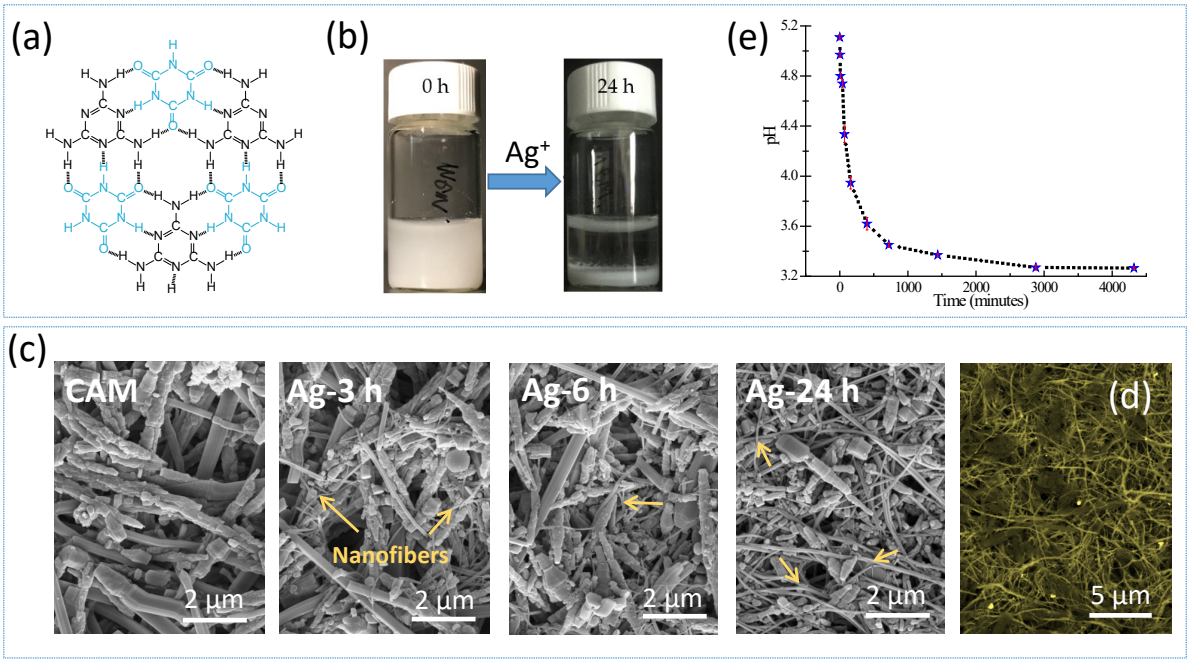

Figure 1. (a) Illustration of the CAM molecular structure. (b) Photos of CAM aqueous suspension and after adding $AgNO_3$ for 24 h. (c) SEM images of CAM and the samples after adding $AgNO_3$ for different time interval. (d) fake-colored back-scattered electron image of sample Ag-24 h. (e) Solution pH change over time after adding $AgNO_3$.

In addition to the morphology and phase variation, another important observation is the decreased pH after the injection of Ag(I) into the solution. The initial pH of the aqueous mixture was 5.11, measured immediately after adding $AgNO_3$ solution into the CAM suspension. We noted the pH dropped to 4.4 after 1 h and then down to 3.37 after standing for 24 h. The pH showed slight decrease upon further standing (up to a week), and eventually stabilized at 3.2 (Figure 1e). These results clearly illustrate the release of protons from the CAM framework during the incorporation of Ag(I). In this context, we assumed that the incomplete transition from CAM nanorods to Ag-contained nanofibers was caused by the high acidity of the reaction mixture. To test this hypothesis, ammonia water (10 vol%) was added to neutralize the protons and hence to promote the recrystallization. As can be clearly seen in Figure 2a, more nanofibers were produced after adding NH_3 for several hours (sample

NH_3-3h and NH_3-5h). After 48 h growth, the sample was exclusively composed of nanofibers (NH_3-48h), with lengths over 1000 μm (Figure S2). In the meantime, the silver concentration in the aqueous solution (denoted as *n*(Ag)) was monitored. As indicated above, the initial *n*(Ag) was set 10 mM, which dropped slightly to 8.49 mM after standing for 24 h (before adding NH_3, Figure 2b). These results suggest that in the absence of NH_3, only a small amount of Ag(I) reacted with CAM nanorods, in accordance with the observation that a small number of nanorods transformed to nanofibers. However, *n*(Ag) dropped dramatically to 1.39 mM 3 hours after adding ammonia and to 0.008 mM after 48 hours, indicating faster and complete reaction of silver ions with CAM. Notably, the final product (NH_3-48h, also denoted CAM-Ag) presents as an integrated, floatable hydrogel membrane (Figure 2b, inset). Upon drying, a free-standing, robust membrane was obtained, featuring a fibrous, multi-layered architecture (Figure 2a). EDS elemental mapping demonstrates homogenous distribution of Ag across the sample (Figure S3).

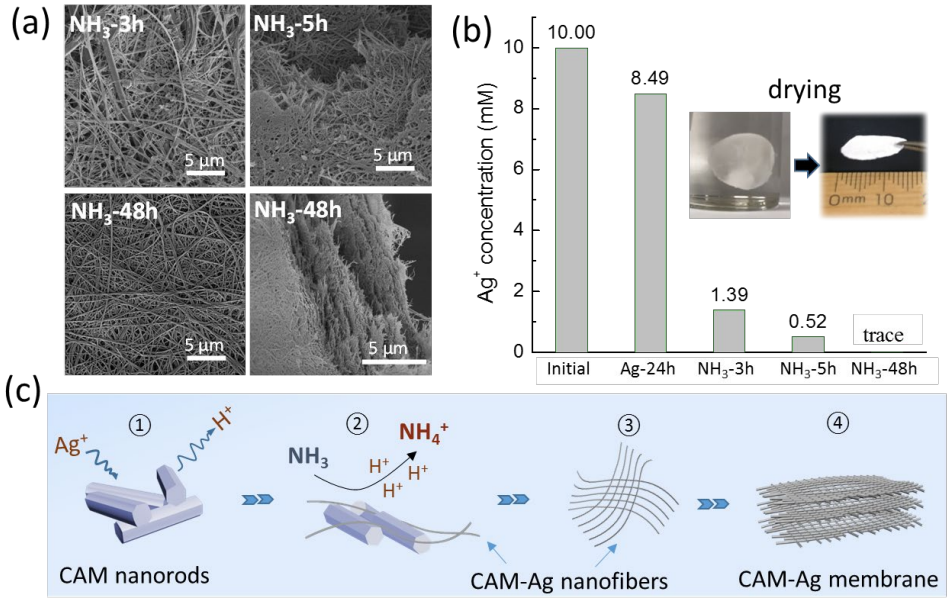

Figure 2. (a) SEM images of NH_3-3h, NH_3-5h, and NH_3-48h. (b) The Ag(I) concentrations in the solution at different stages: initial, after adding Ag(I) for 24 h and after adding ammonia for 3, 5 and 48 h. (c) Schematic representation of the CAM to CAM-Ag transformation and the formation of the free-standing supramolecular membrane.

To better understand the transformation from CAM nanorods to CAM-Ag nanofibers, a schematic illustration of the process is proposed (Figure 2c). Upon adding Ag(I) into the suspension of the CAM crystals, the protons in CAM molecules are activated and liberated into the solution, meanwhile with the Ag incorporated into the supramolecular framework (Stage ①). This process leads to the conversion from CAM to CAM-Ag, associated with the morphology changing from nanorods to nanofibers. However, the reaction is suspended when the pH is too low (≈3), reflected by the observation that only a small portion of nanorods spontaneously convert into nanofibers. Addition of ammonia neutralizes the protons generated by silver coordination, driving the equilibrium towards the formation of CAM-Ag (Stage ②). Finally, the nanorods completely transform to nanofibers, with all the Ag(I) incorporated into the supramolecular structure (Stage ③). Interestingly, the CAM-Ag nanofibers obtained interlink with each other and self-assemble into a multi-layered hydrogel membrane (Stage ④), which transform into a self-supported, millimeter-sized membrane after drying.

2.2. Insights into structural evolution of the supramolecular framework

The structural evolution of the supramolecular framework from CAM to CAM-Ag was investigated using a range of different techniques. As briefly mentioned above, the structural evolution was firstly monitored by PXRD. In the diffraction pattern of CAM (Figure 3a), the peak at 10.9° (2θ) corresponds to the in-plane structural packing motif of hexagonal units with a distance of ca. 0.83 nm.[26, 34-35] The characteristic diffraction peak at 27.9° reveals the inter-planar stacking distance of 0.32 nm.[26, 34-35] Twenty four hours after the addition of Ag(I) (sample Ag-24h), new diffraction peaks appeared at 12.5, 18.6 and 31.3°, indicating the formation of a new crystal phase upon the reaction with silver. After adding ammonia, these new peaks intensified further and became most pronounced for sample NH_3-48h (Figure 3a). Notably, the diffraction peak of the CAM-Ag at 6.28° corresponds to a spacing of 1.40 nm

and indicates a lamellar structure of the nanofibers, which was confirmed by high-resolution TEM (Figure S4). The PXRD spectra of the samples (except CAM) were obtained by directly measuring the integral membranes. When measuring the ground powder of NH_3-48h instead several other peaks emerged, including a large peak at 10.9° suggesting the nanofibers in NH_3-48h are crystallographically oriented. Synchrotron radiation was used to solve the single crystal structure of the final CAM-Ag product as discussed below.

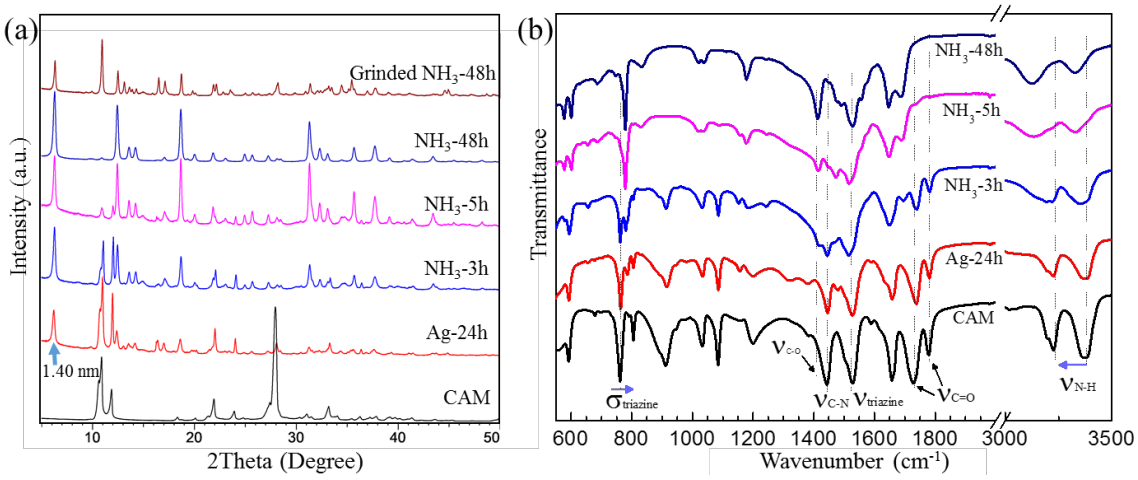

Figure 3. (a) PXRD patterns and (b) IR spectra of the pristine CAM nanorods, after reacting with Ag(I) for 24 h, and those after adding ammonia for different time.

Infrared (IR) spectroscopy was employed to study the chemical structures (Figure 3b). For the CAM sample, the bands located at 1728 and 1779 cm^{-1} correspond to the stretching modes of the carbonyl group in *keto*-CA ($\nu_{C=O}$).[36-37] The absorption peak at 1442 cm^{-1} was assigned to the stretching of CN-heterocycles (ν_{C-N}). After adding Ag(I) and ammonia, the stretching bands of $\nu_{C=O}$ and ν_{C-N} in CAM weakened and finally vanished (sample Ag-24h to NH_3-48h). These results, together with the appearance of a new band at 1414 cm^{-1} which is related to C-O vibration, strongly indicate the tautomerization of CA from *keto*-type to *enol*-type.[36-37] Additionally, the stretching vibration band of the amino group (ν_{N-H}) in CAM-Ag located at 3200-3400 cm^{-1} shifts to lower wavenumbers compared to CAM, which is believed to result from the strengthening of the O···H-N hydrogen bond in CAM-Ag.[38-40] The

vibration band at 1528 cm^{-1}, which is assigned to the stretching mode of the triazine units ($\nu_{triazine}$), became broader for CAM-Ag, most likely owing to the formation of N-Ag-N coordinate bonds. The breathing mode of triazine units ($\sigma_{triazine}$) shifted from 762 to 779 cm^{-1}, also resulting from the *keto*-to-*enol* tautomerization of CA. It is worthwhile to mention that without adding Ag(I), ammonia alone was unable to trigger the tautomerization, as indicated by IR spectra (Figure S5), implying that the reaction with Ag(I) was the driving force for the conversion, rather than the basic environment.

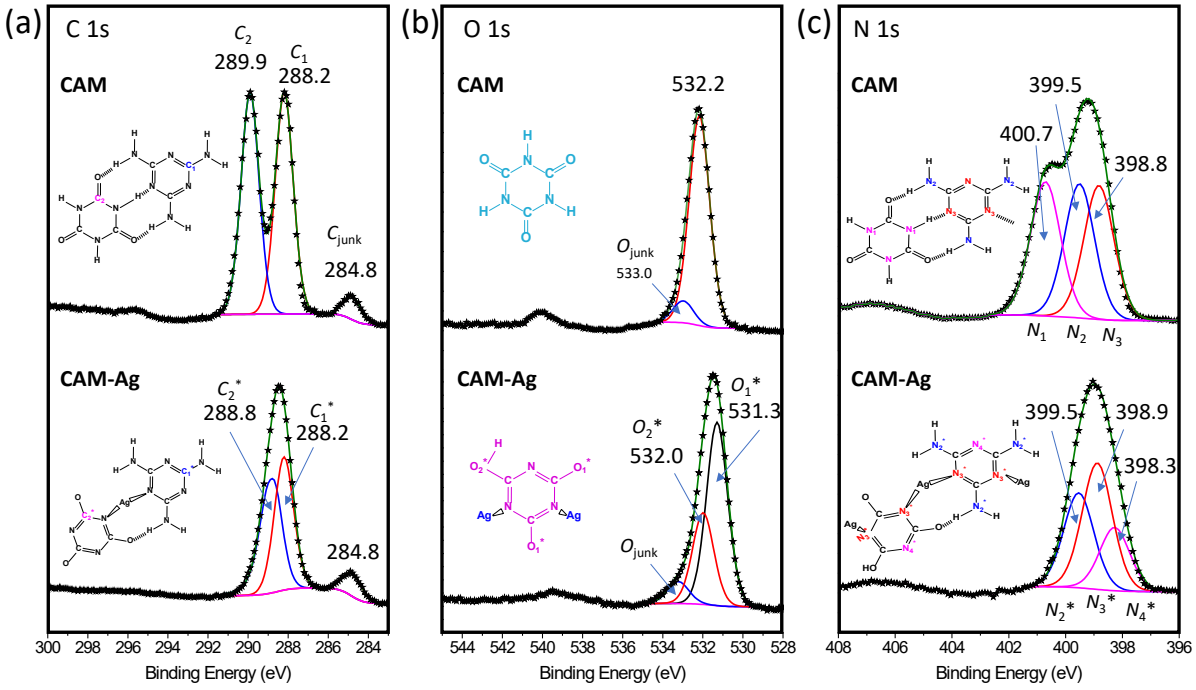

Figure 4. XPS spectra of sample CAM and CAM-Ag: (a) C 1s band, (b) O 1s band, and (c) N 1s band. Star-lines indicate raw data.

The tautomerization related structural variation is further verified by X-ray photoelectron spectroscopy (XPS). For the C 1s spectrum of CAM (Figure 4a), the two peaks at 288.2 eV and 289.9 eV are attributed to the C atoms in the triazine ring (N-C=N, C_1) in M and the heterocycle in *keto*-CA (O=C-N, C_2), respectively. The peak at 284.8 eV is ascribed to adventitious hydrocarbon. For CAM-Ag, the corresponding C_1^* peak is located at the same

position as C_1, resulting from the intact melamine molecules. C_2^* shifted significantly to a lower binding energy of 288.8 eV compared to C_2, suggesting the transformation from O=C-N (*keto*-CA) to O-C=N (*enol*-CA). The O 1s spectra of CAM is located at 532.2 eV, with the one at 533.0 eV arising from environmental oxygen (Figure 4b). The O 1s spectra of CAM-Ag, on the other hand, was fitted into two peaks at 531.3 eV (O_1*) and 532.0 eV (O_2*) with an area ratio of 2:1 (environmental oxygen excluded), representing the enolate-oxygen and enol-oxygen, in accordance with the tautomerization conversion of C=O to C-O bond during which two of the hydrogens has been replaced by Ag(I). In terms of the N 1s spectrum for CAM (Figure 4c), it can be deconvoluted into three peaks at 400.7, 399.5, and 398.8 eV, which are assigned to the N-heterocyclic rings (C-NH-C, N_1), amines (H_2N-C, N_2), and triazine (C=N-C, N_3), respectively.[41] The N 1s spectrum of CAM-Ag was deconvoluted to three peaks at 399.5, 398.9, and 398.3 eV, which correspond to the N atoms in the amines (H_2N-C, N_2^*), Ag~triazine (C=N(Ag)-C, N_3^*) and triazine (C=N-C, N_4^*). The disappearance of N_1 binding energy (C-NH-C) was also indicative of the resonance structural transformation of CA. The crystal transformation from CAM to CAM-Ag can be attributed to the formation of relatively stronger N-Ag-N coordinate bonds than the hydrogen bonds. The XPS measurements, along with the XRD and IR results, provided insights into the structural transformation and were also helpful for determining the single-crystal structure of CAM-Ag.

2.3. Single crystal structure of the CAM-Ag nanofiber

Highly crystalline CAM-Ag nanofibers were separated and collected and appeared to be single crystalline under optical microscopy (Figure S6). The nanofiber afforded a discrete diffraction pattern using a synchrotron X-ray source, which allowed for the unambiguous determination of connectivity. The crystal structure was solved and refined in the space group *P*1, with the asymmetric unit containing eight silver atoms, four melamine and four cyanuric acid molecules, (Table S1). The empirical formula of $[CA_4\text{-}M_4\text{-}Ag_8]_n$ can be derived, in

accordance with the original molecular ratio of CAM and Ag. In addition to the CAM-Ag complex, regions of diffuse electron density for which an appropriate disorder model could not be derived were observed. This was masked using PLATON SQUEEZE,[42] which removed electron density corresponding to 142 electrons per unit cell (approximately 7.9 water molecules). The correctness of the final refined structural model for CAM-Ag is indubitable as the simulated PXRD spectrum matches very well with its measured pattern (Figure 5a).

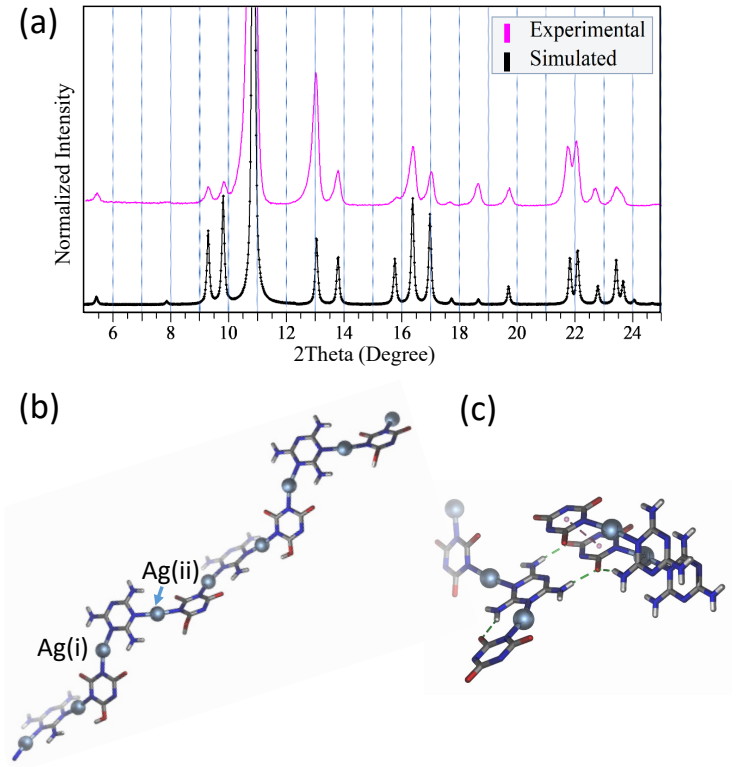

Figure 5. (a) PXRD spectra of the CAM-Ag single fibers based on experiment and simulation; (b) A unit of the CAM-Ag single-crystal structure showing one-dimensional coordination polymer chain; (c) Selected principal supramolecular interactions in the single crystal structure of CAM-Ag: hydrogen bonds shown in green and π-π interactions in red.

As shown in Figure 5b, CAM-Ag is a 1D coordination polymer consisting of alternating melamine and dianionic cyanurate (*enol*-type) ligands linked via silver coordination {Ag-M-

Ag-CA-Ag-M)$_n$. There are two types of silver coordinate bonds: one links the M and CA in a slightly distorted planar configuration (Ag(i)), constituting the building unit of (M-Ag-CA); the other one, links the units in a twisted motif ((M-Ag-CA)-Ag-(M-Ag-CA)-Ag-(M-Ag-CA)), forming a helical chain conformation (Ag(ii)). Each chain is associated with adjacent chains by a series of hydrogen bonds and π-π interactions (Figure 5c). Key among these is the complementary melamine-cyanuric acid triple H-bond motif observed between each non-coordinating edge of each ligand (average H···A distance 2.02 Å), forming an undulating 2D sheet. Additional N-H···O hydrogen bonds (2.056, 2.063 Å) link to adjacent sheets, causing formation of a 3D hydrogen bonded network. Each chain also interacts with those directly above and below via π-π interactions (3.471 Å). A further stabilizing intra-chain N-H···O hydrogen bond (average 2.27 Å) occurs between each crystallographically independent CA-M pair. An overview of the CAM-Ag crystal structure is illustrated in Figure 6.

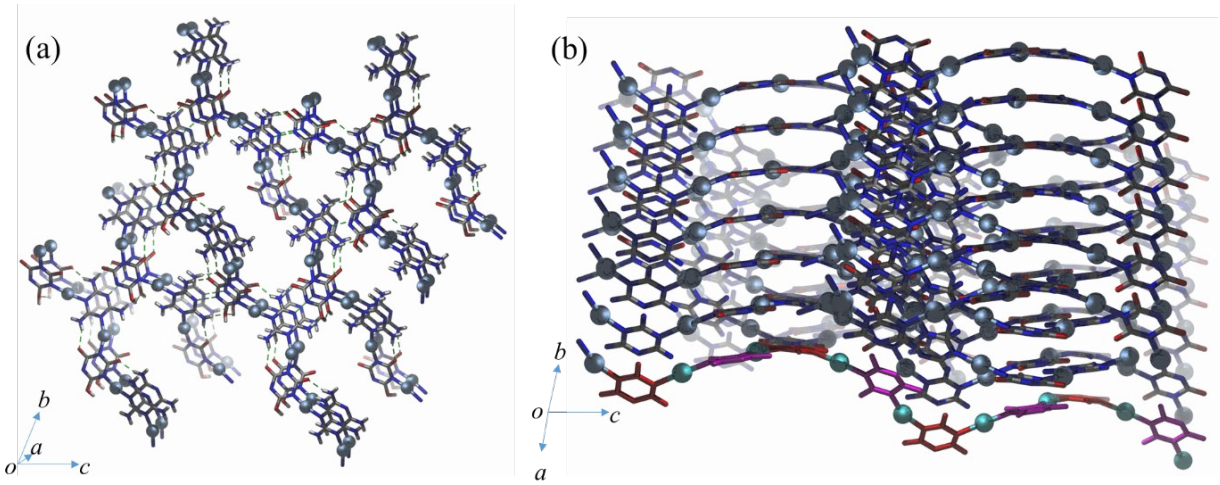

Figure 6. Overview of the CAM-Ag crystal structure showing the undulating 2D layer (a) view towards [100] direction (slightly tilted) and (b) view towards [120] direction. The outside chain is colored differently for better visualization.

2.4. Mechanical strength and optical transmittance of the CAM-Ag membrane

The macroscale, free-standing supramolecular membrane assembled by CAM-Ag nanofibers exhibits remarkable stability, flexibility and high accessibility. As can be seen in

Figure S7, the XRD patterns of the membranes after standing for 7 days and 6 months in air at ambient conditions demonstrate very minor difference from the pattern of the freshly prepared membrane. Powder XRD patterns of the membrane upon heating were also collected (Figure S8), which reveal that the membrane retained the crystal structures up to 150 ºC or even 200 ºC, indicating good stability at elevated temperatures.

As to mechanical strength, the membrane can be bent over 90º by fingers and then fully recover for many cycles (inset in Figure 7a). Nanoindentation technique was first employed for mechanical tests. The reduced modulus of sample Ag-24h was measured to be 590.7 MPa (Figure 7a), but large variations were observed across the sample owing to the presence of heterogenous materials and morphologies, as aforementioned. For the membranes obtained after adding ammonia, the modulus decreased significantly to 159.5 MPa for NH_3-3h, and down to 116.1 and 57.6 MPa for NH_3-5h and NH_3-48h, respectively, meanwhile becoming very uniform for these samples. Tensile tests show that the bulk membrane had a Young's modulus of 77 ± 10 MPa and an elongation of 3.4 ± 0.5. The tensile strength was determined to be 2.2 ± 0.2 MPa (Table S2). A representative strain-stress curve is shown in Figure S9. These results are comparable to the performances of films made of small organic molecules[22] and nonwoven polymer fibers.[43] We considered that the macroscopic flexibility of the membrane is related to the mechanical property of the CAM-Ag nanofibers. In this sense, the three-point bending test was performed by nanoindentation to assess the bending stiffness of single CAM-Ag and CAM fibers. As schematically shown in Figure 7b, the fiber was suspended on top of square hole and fixed at the ends by super glue, and a conical indenter was used for the measurement. The bending stiffness was determined to be 12.1 N/m for CAM-Ag and 18.6 N/m for CAM. The failure force for CAM-Ag and CAM was 231.2 μN at 15.5 μm displacement and 91.1 μN at 3.1 μm displacement, respectively (Figure 7c). These

results clearly illustrate the enhanced flexibility of CAM-Ag than that of CAM, which should be assigned to its 1D coordination polymer chains in comparison to CAM's planer structure.

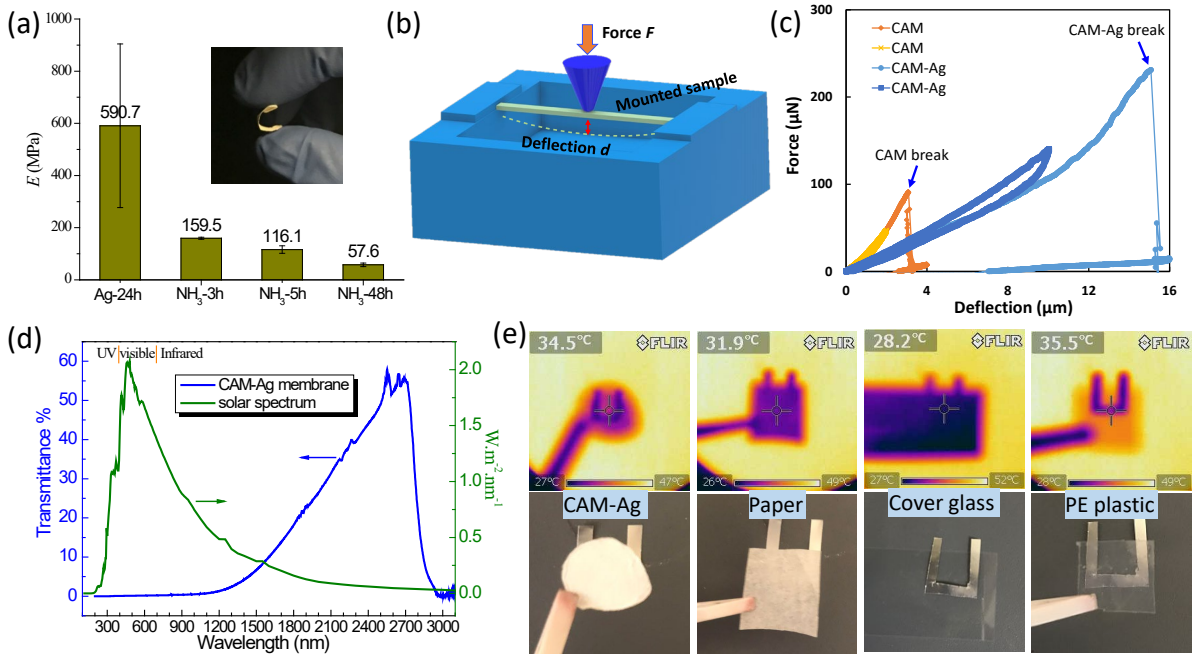

Figure 7. (a) Reduced modulus of membranes made of Ag-24h, NH_3-3h, NH_3-5h and NH_3-48h (CAM-Ag). Inset: CAM-Ag membrane bent by fingers. (b) Schematic of the 3-point bending test on single fiber. (c) Force-deflection curves of CAM and CAM-Ag fibers from 3-point bending test. (d) UV-vis-IR spectrum of CAM-Ag membrane. (e) Exhibitions of CAM-Ag membrane showing optical opaque but IR transparency with a thermal camera, cellulose paper being both optical and IR opaque, cover glass being optical transparent but IR opaque, and PE plastic being both optical and IR transparent.

Remarkably, the CAM-Ag membrane demonstrates selective light transmission. As shown in the transmittance spectrum (Figure 7d), the CAM-Ag membrane had almost no transmission in the range of UV, visible and near-IR light (200-1100 nm). Nevertheless, a transmission window in the shortwave IR range was observed (1500 to 2900 nm), with maximum transparency above 50% in the band of 2500-2700 nm. The diffuse reflectance spectrum of the membrane (Figure S10) shows that the opacity in UV is mostly due to

absorption while the non-transmittance for visible light is largely due to reflection. The optical transmission is distinct from commonly used materials. For a more visible comparison, the transmittance over the vis/IR range of the CAM-Ag membrane and several materials was monitored by thermal imaging. By covering the lens with a CAM-Ag membrane, the thermal camera still clearly captured the image of the heated U-shaped foil underneath, illustrating that the IR light crossed the membrane (Figure 7e). The light transmittance of the membrane is distinct compared to paper made from cellulose pulp which blocks both visible and IR light; cover-slip glass is visually transparent but IR opaque, while polyethylene cling wrap is transparent in both visual and IR regions. More work is undertaken to understand the unique electromagnetic transmission of the CAM-Ag membrane, which indicates promising applications in important areas such as optical windows and textile for radiative cooling.[44-45]

3. Conclusions

We have demonstrated a facile approach for the synthesis of a robust, free-standing, centimeter-sized supramolecular membrane through competitive incorporation of Ag(I) into the hydrogen-bonded CAM network. By simply injecting Ag(I) into the aqueous dispersion of CAM nanorods, two in three of protons from cyanuric acid were replaced by Ag(I) and liberated to the solution. The silver ions incorporated into the framework forming coordinate bonds with the nitrogen atoms alternatingly from melamine and cyanuric acid. The resulting crystal transition had to be facilitated by ammonia, which neutralized the excess protons and resulted in the complete transformation of CAM nanorods to CAM-Ag nanofibers, a new type of supramolecular crystal, associated with the *keto*-to-*enol* tautomerisation of cyanuric acid. The single crystal structure of the CAM-Ag nanofiber was solved in space group *P*1, featuring helical chains of $(\text{Ag-M-Ag-CA-Ag-M})_n$ by coordinate bonding. Hydrogen bonds are formed between the chains, resulting in undulating 2D sheets which then generate stacked layers in the 3D by the formation of interlayer π-π interactions. Significantly, the nanofibers

self-assembled into a free-standing membrane with strong macroscopic robustness, allowing for easy handling and high processibility. The supramolecular membranes show unique optical transmittance that the membranes only allow for the transmission of shortwave IR light, while UV-visible light is fully reflected or absorbed. These findings shed light on the interplays between different non-covalent interactions (coordinate bonds, hydrogen bonds, *van der Waals* force, etc), which may act as a toolbox for fabricating new 2D supramolecular materials with distinct functionalities.

■ ASSOCIATED CONTENT

Supporting Information

Experimental details for materials synthesis; instrumentation; nanoindentation measurements; SEM and TEM images; FTIR spectra; PXRD pattern; X-ray crystallographic data. This material is available free of charge via the Internet at http://pubs.acs.org.

■ AUTHOR INFORMATION

Corresponding author

*Email : Jingsan.Xu@qut.edu.au

Notes

The authors declare no conflict of interest.

■ ACKNOWLEDGMENTS

The authors acknowledge the financial support by the Australian Research Council. Science and Engineering Faculty and Central Analytical Research Facility (CARF) at QUT are greatly acknowledged for technical assistance. The single crystal X-ray diffraction pattern was collected on the MX2 beamline at the Australian Synchrotron, part of ANSTO. We thank the Synchrotron for travel funding and the beamline staff for their assistance.

■ REFERENCE

1. Atwood, J.; Gokel, G.; Barbour, L. *Comprehensive supramolecular chemistry II*; Elsevier: Oxford, 2017.

2. Liu, M.; Zhang, L. Y.; Hua, Y.; Feng, L. P.; Jiang, Y.; Ding, X. J.; Qi, W.; Wang, H. Mesoporous Silver Melamine Nanowires Formed by Controlled Supermolecular Self-Assembly: A Selective Solid-State Electroanalysis for Probing Multiple Sulfides in Hyperhaline Media through the Specific Sulfide Chloride Replacement Reactions. *Anal. Chem.* **2017,** *89*, 9552-9558.
3. Liu, K.; Kang, Y.; Wang, Z.; Zhang, X. 25th Anniversary Article: Reversible and Adaptive Functional Supramolecular Materials: "Noncovalent Interaction" Matters. *Adv. Mater.* **2013,** *25*, 5530-5548.
4. Huang, Z.; Zhang, M.; Lin, H.; Ding, S.; Dong, B.; Liu, D.; Wang, H.; Dai, F.; Sun, D. Comparison of two water oxidation electrocatalysts by copper or zinc supermolecule complexes based on porphyrin ligand. *RSC Adv.* **2018,** *8*, 40054-40059.
5. Qiu, S.; Hou, Y.; Xing, W.; Ma, C.; Zhou, X.; Liu, L.; Kan, Y.; Yuen, R. K. K.; Hu, Y. Self-assembled supermolecular aggregate supported on boron nitride nanoplatelets for flame retardant and friction application. *Chem. Eng. J.* **2018,** *349*, 223-234.
6. Lin, C. M.; Li, M. S.; Dwivedi, A. K.; Lin, H. C. Synthesis and enhanced electron transfer of supramolecular nano-composite containing dendritic dye and surface-modified ZnO nano-rods. *Dyes Pigments* **2018,** *157*, 179-189.
7. Yang, F.; Tao, F.; Li, C.; Gao, L.; Yang, P. Self-assembled membrane composed of amyloid-like proteins for efficient size-selective molecular separation and dialysis. *Nat. Commun.* **2018,** *9*, 5443.
8. Miller, D. J.; Dreyer, D. R.; Bielawski, C. W.; Paul, D. R.; Freeman, B. D. Surface Modification of Water Purification Membranes. *Angew. Chem. Int. Edit.* **2017,** *56*, 4662-4711.
9. Zha, R. H.; Sur, S.; Stupp, S. I. Self-assembly of Cytotoxic Peptide Amphiphiles into Supramolecular Membranes for Cancer Therapy. *Adv. healthcare mater.* **2013,** *2*, 126-133.
10. Dong, R.; Pfeffermann, M.; Liang, H.; Zheng, Z.; Zhu, X.; Zhang, J.; Feng, X. Large-Area, Free-Standing, Two-Dimensional Supramolecular Polymer Single-Layer Sheets for Highly Efficient Electrocatalytic Hydrogen Evolution. *Angew. Chem. Int. Edit.* **2015,** *54*, 12058-12063.
11. Zhuang, X.; Mai, Y.; Wu, D.; Zhang, F.; Feng, X. Two-dimensional soft nanomaterials: a fascinating world of materials. *Adv. Mater.* **2015,** *27*, 403-427.
12. Yu, H.; Qiu, X.; Moreno, N.; Ma, Z.; Calo, V. M.; Nunes, S. P.; Peinemann, K. V. Self-Assembled Asymmetric Block Copolymer Membranes: Bridging the Gap from Ultra- to Nanofiltration. *Angew. Chem. Int. Edit.* **2015,** *54*, 13937-13941.
13. Cheng, C. C.; Chiu, T. W.; Yang, X. J.; Huang, S. Y.; Fan, W. L.; Lai, J. Y.; Lee, D. J. Self-assembling supramolecular polymer membranes for highly effective filtration of water-soluble fluorescent dyes. *Polym. Chem.* **2019,** *10*, 827-834.
14. Krieg, E.; Weissman, H.; Shirman, E.; Shimoni, E.; Rybtchinski, B. A recyclable supramolecular membrane for size-selective separation of nanoparticles. *Nat. Nanotechnol.* **2011,** *6*, 141.
15. Beginn, U.; Zipp, G.; Möller, M. Functional Membranes Containing Ion-Selective Matrix-Fixed Supramolecular Channels. *Adv. Mater.* **2000,** *12*, 510-513.
16. Liang, B.; Wang, H.; Shi, X.; Shen, B.; He, X.; Ghazi, Z. A.; Khan, N. A.; Sin, H.; Khattak, A. M.; Li, L.; Tang, Z. Microporous membranes comprising conjugated polymers with rigid backbones enable ultrafast organic-solvent nanofiltration. *Nat. Chem.* **2018,** *10*, 961–967.
17. Pfeffermann, M.; Dong, R.; Graf, R.; Zajaczkowski, W.; Gorelik, T.; Pisula, W.; Narita, A.; Müllen, K.; Feng, X. Free-standing monolayer two-dimensional supramolecular organic framework with good internal order. *J. Am. Chem. Soc.* **2015,** *137*, 14525-14532.
18. Kambe, T.; Sakamoto, R.; Hoshiko, K.; Takada, K.; Miyachi, M.; Ryu, J. H.; Sasaki, S.; Kim, J.; Nakazato, K.; Takata, M.; Nishihara, H. π-Conjugated Nickel Bis(dithiolene) Complex Nanosheet. *J. Am. Chem. Soc.* **2013,** *135*, 2462-2465.
19. Huang, X.; Li, H.; Tu, Z.; Liu, L.; Wu, X.; Chen, J.; Liang, Y.; Zou, Y.; Yi, Y.; Sun, J.; Xu, W.; Zhu, D. Highly Conducting Neutral Coordination Polymer with Infinite Two-Dimensional Silver–Sulfur Networks. *J. Am. Chem. Soc.* **2018,** *140*, 15153-15156.
20. Schrettl, S.; Stefaniu, C.; Schwieger, C.; Pasche, G.; Oveisi, E.; Fontana, Y.; Morral, A. F. i.; Reguera, J.; Petraglia, R.; Corminboeuf, C.; Brezesinski, G.; Frauenrath, H. Functional carbon nanosheets prepared from hexayne amphiphile monolayers at room temperature. *Nat. Chem.* **2014,** *6*, 468.

21. Niazov-Elkan, A.; Sui, X.; Kaplan-Ashiri, I.; Shimon, L. J. W.; Leitus, G.; Cohen, E.; Weissman, H.; Wagner, H. D.; Rybtchinski, B., Modular Molecular Nanoplastics. *ACS Nano* **2019**, 13, 11097-11106.
22. Wolf, T.; Niazov-Elkan, A.; Sui, X.; Weissman, H.; Bronshtein, I.; Raphael, M.; Wagner, H. D.; Rybtchinski, B., Free-Standing Nanocrystalline Materials Assembled from Small Molecules. *J. Am. Chem. Soc.* **2018**, 140, 4761-4764.
23. Seto, C. T.; Whitesides, G. M. Molecular self-assembly through hydrogen bonding: supramolecular aggregates based on the cyanuric acid-melamine lattice. *J. Am. Chem. Soc.* **1993,** *115*, 905-916.
24. Ranganathan, A.; Pedireddi, V.; Rao, C. Hydrothermal synthesis of organic channel structures: 1: 1 hydrogen-bonded adducts of melamine with cyanuric and trithiocyanuric acids. *J. Am. Chem. Soc.* **1999,** *121*, 1752-1753.
25. Roy, B.; Bairi, P.; Nandi, A. K. Supramolecular assembly of melamine and its derivatives: nanostructures to functional materials. *RSC Adv.* **2014,** *4*, 1708-1734.
26. Shalom, M.; Inal, S.; Fettkenhauer, C.; Neher, D.; Antonietti, M. Improving Carbon Nitride Photocatalysis by Supramolecular Preorganization of Monomers. *J. Am. Chem. Soc.* **2013,** *135*, 7118-7121.
27. Shalom, M.; Guttentag, M.; Fettkenhauer, C.; Inal, S.; Neher, D.; Llobet, A.; Antonietti, M. In situ formation of heterojunctions in modified graphitic carbon nitride: Synthesis and noble metal free photocatalysis. *Chem. Mater.* **2014,** *26*, 5812-5818.
28. Shalom, M.; Gimenez, S.; Schipper, F.; Herraiz-Cardona, I.; Bisquert, J.; Antonietti, M. Controlled Carbon Nitride Growth on Surfaces for Hydrogen Evolution Electrodes. *Angew. Chem.* **2014,** *126*, 3728-3732.
29. Wang, J.; Cong, J.; Xu, H.; Wang, J.; Liu, H.; Liang, M.; Gao, J.; Ni, Q.; Yao, J. Facile Gel-Based Morphological Control of Ag/g-C_3N_4 Porous Nanofibers for Photocatalytic Hydrogen Generation. *Acs Sustain. Chem. Eng.* **2017,** *5*, 10633-10639.
30. Bairi, P.; Roy, B.; Nandi, A. K. PH and anion sensitive silver(i) coordinated melamine hydrogel with dye absorbing properties: Metastability at low melamine concentration. J. *Mater. Chem.* **2011,** *21*, 11747-11749.
31. Fei, J.; Gao, L.; Zhao, J.; Du, C.; Li, J. Responsive Helical Self-Assembly of $AgNO_3$ and Melamine Through Asymmetric Coordination for Ag Nanochain Synthesis. *Small* **2013,** *9*, 1021-1024.
32. Beatty, A. M. Hydrogen bonded networks of coordination complexes. *Cryst. Eng. Comm.* **2001,** *3*, 243-255.
33. García-Zarracino, R.; Höpfl, H. A 3D Hybrid Network Containing Large Spherical Cavities Formed through a Combination of Metal Coordination and Hydrogen Bonding. *Angew. Chem. Int. Edit.* **2004,** *43*, 1507-1511.
34. Jun, Y. S.; Park, J.; Lee, S. U.; Thomas, A.; Hong, W. H.; Stucky, G. D. Three-Dimensional Macroscopic Assemblies of Low-Dimensional Carbon Nitrides for Enhanced Hydrogen Evolution. *Angew. Chem.* **2013,** *125*, 11289-11293.
35. Tong, Z.; Yang, D.; Sun, Y.; Nan, Y.; Jiang, Z. Tubular g-C_3N_4 Isotype Heterojunction: Enhanced Visible-Light Photocatalytic Activity through Cooperative Manipulation of Oriented Electron and Hole Transfer. *Small* **2016,** *12*, 4093-101.
36. Szczepaniak, K.; Szczesniak, M. Matrix isolation infrared studies of nucleic acid constituents: Part 4. Guanine and 9-methylguanine monomers and their keto—enol tautomerism. *J. Mol. Struct.* **1987,** *156*, 29-42.
37. Nowak, M. J.; Lapinski, L.; Fulara, J. Matrix isolation studies of cytosine: The separation of the infrared spectra of cytosine tautomers. *Spectrochim. Acta. A* **1989,** *45*, 229-242.
38. ASKOUNI, I. M. K. A. T. Absorption Spectra and Tautomerism of Cyanuric Acid, Melamine and Some Related Compounds. *J. Am. Chem. Soc.* **1947,** *69*, 801-803.
39. Seifer, G. B. J. R. J. O. C. C. Cyanuric Acid and Cyanurates. *Russ. J. Coord. Chem.* **2002,** *28*, 301-324.
40. Liang, X. Q.; Pu, X. M.; Zhou, H. W.; Wong N. B.; Tian, A. M. Keto–enol tautomerization of cyanuric acid in the gas phase and in water and methanol. *J. Mol. Struc. Theochem* **2007,** *816*, 125-136.

41. Kundu, S.; Xia, W.; Busser, W.; Becker, M.; Schmidt, D. A.; Havenith, M.; Muhler, M. The formation of nitrogen-containing functional groups on carbon nanotube surfaces: a quantitative XPS and TPD study. *Phys. Chem. Chem. Phys.* **2010,** *12*, 4351-4359.
42. Spek, A. L. PLATON SQUEEZE: a tool for the calculation of the disordered solvent contribution to the calculated structure factors. *Acta. Crystallogr. C* **2015,** *71*, 9-18.
43. Carrizales, C.; Pelfrey, S.; Rincon, R.; Eubanks, T. M.; Kuang, A.; McClure, M. J.; Bowlin, G. L.; Macossay, J. Thermal and mechanical properties of electrospun PMMA, PVC, Nylon 6, and Nylon 6,6. *Polym. Adv. Technol.* **2008**, 19, 124-130.
44. Hsu, P.C.; Liu, C.; Song, A. Y.; Zhang, Z.; Peng, Y.; Xie, J.; Liu, K.; Wu, C.L.; Catrysse, P. B.; Cai, L.; Zhai, S.; Majumdar, A.; Fan, S.; Cui, Y. A dual-mode textile for human body radiative heating and cooling. *Sci. Adv.* **2017**, 3, e1700895.
45. Hsu, P.-C.; Song, A. Y.; Catrysse, P. B.; Liu, C.; Peng, Y.; Xie, J.; Fan, S.; Cui, Y., Radiative human body cooling by nanoporous polyethylene textile. *Science* **2016**, 353, 1019-1023.

For Table of Contents Only